Eur. Phys. J. B **18**, 215–225 (2000)

THE EUROPEAN PHYSICAL JOURNAL B

EDP Sciences

Doping-dependent electronic structure of cuprates studied using angle-scanned photoemission

P. Schwaller[1,a], T. Greber[1], P. Aebi[2], J.M. Singer[1], H. Berger[3], L. Forró[4], and J. Osterwalder[1,b]

[1] Physik-Institut der Universität Zürich, Winterthurerstrasse 190, 8057 Zürich, Switzerland
[2] Institut de Physique, Université de Fribourg, 1700 Fribourg, Switzerland
[3] Institut de Physique Appliquée, EPFL, 1015 Lausanne, Switzerland
[4] DP/IGA, EPFL, 1015 Lausanne, Switzerland

Received 12 October 1999 and Received in final form 12 April 2000

Abstract. Full $\mathbf{k}_{\|}$-maps of the electronic structure near the Fermi level of differently doped cuprates measured with angle-scanned photoelectron spectroscopy are presented. The valence band maximum of the antiferromagnetic insulator $Sr_2CuO_2Cl_2$, which is taken as a representative of an undoped cuprate, and the Fermi surfaces of overdoped, optimally doped and underdoped $Bi_2Sr_2CaCu_2O_{8+\delta}$ high-temperature superconductors are mapped in the normal state. The results confirm the existence of large Luttinger Fermi surfaces at high doping with a Fermi surface volume proportional to $(1+x)$, where x is the hole concentration. At very low doping, however, we find that this assumption based on Luttinger's theorem is not fulfilled. This implies a change in the topology of the Fermi surface. Furthermore the intensity of the *shadow bands* observed on the Fermi surface of $Bi_2Sr_2CaCu_2O_{8+\delta}$ as a function of the doping is discussed.

PACS. 79.60.-i Photoemission and photoelectron spectra – 74.25.Jb Electronic structure – 71.18.+y Fermi surface: calculations and measurements; effective mass, g factor

1 Introduction

A detailed knowledge of the normal-state electronic structure of hole-doped cuprates is important for the understanding of the mechanism of high-temperature superconductivity. Currently the topology and the volume of the normal-state Fermi surface at different hole concentrations are in the center of discussion.

Angle-resolved ultraviolet photoelectron spectroscopy (ARUPS) is a suitable tool to investigate the Fermi surface of cuprates [1,2]. The standard way to determine the Fermi surface with ARUPS is to measure energy distribution curves $E(\mathbf{k})$ at different $\mathbf{k}$-locations, *i.e.* at different emission angles or photon energies, and to determine the $\mathbf{k}$-locations where occupied bands cross E_F [1,2]. Whereas such $E(\mathbf{k})$ measurements can be done with an energy resolution of some ten meV, only very few $\mathbf{k}$-locations along some high-symmetry directions are usually probed, which makes an evaluation of tiny features rather difficult. An alternative approach, which we apply in our experiments, is to fix the electron analyzer energy at E_F and to scan at this energy a large number of emission angles. In complement to the $E(\mathbf{k})$ method it seems appropriate to call this the $\mathbf{k}(E)$ mode. At $\mathbf{k}$-locations where direct transitions at E_F occur high photoelectron intensities are expected. The $\mathbf{k}(E)$ mode provides reliable Fermi surface locations even with moderate energy resolutions as long as the dispersive features are not very flat near E_F. Figure 1 sketches the $\mathbf{k}(E)$ mode measuring procedure for the example of an optimally doped $Bi_2Sr_2CaCu_2O_{8+\delta}$ (Bi2212) sample. A series of energy distribution curves measured along a Fermi surface crossing at a polar photoelectron emission angle of 39° are presented. In Figure 1 spectra for azimuthal angles going from 26° to 43° are shown. The 0° reference is located on the line connecting the $(0,0)$ and (π,π) points (see also Fig. 4). The vertical dashed lines indicate the energy window for a $\mathbf{k}(E_F)$ scan. The intensities measured within this window for these spectra are shown in the inset in the lower right corner of Figure 1. One finds that the maximum intensity (spectrum measured at 33°) within the measuring window occurs near the Fermi level crossing [3]. The $\mathbf{k}(E)$ mode was first applied by Santoni *et al.* [4]. They mapped the Fermi surface of layered graphite with a two-dimensional display-type analyzer. We use a sequential angle-scanning data acquisition with a conventional angle-resolving analyzer which provides a much higher signal-to-background ratio and better energy- and angular resolution than a display-type analyzer [5]. Mapping the photocurrent at E_F as a function of $k_{\|}$, the parallel component of the photoelectron wavevector, one obtains intensity contours which are

[a] *Present address:* Institut de Physique, Université de Fribourg, 1700 Fribourg, Switzerland
[b] e-mail: osterwal@physik.unizh.ch

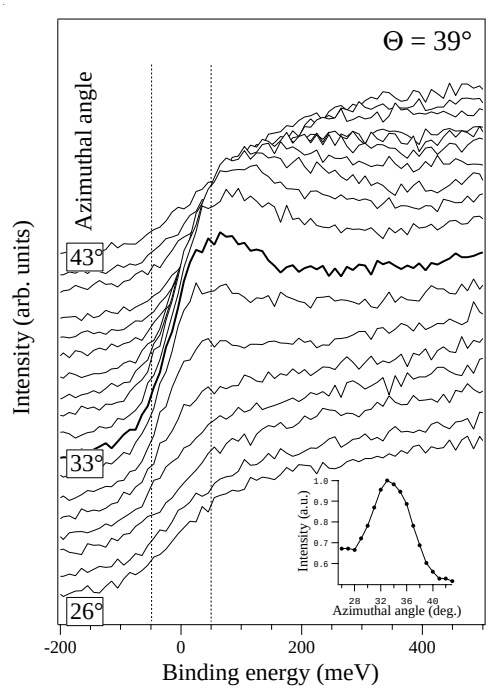

Fig. 1. Energy distribution curves for a polar photoelectron emission angle of 39° off normal along a Fermi surface crossing of optimally doped Bi2212 measured with 21.22 eV photons. The dashed vertical lines indicate the measuring window for a Fermi surface measurement (see text). The inset shows the intensities measured within this measuring window for these spectra. The maximum intensity (spectrum measured at 33°) within the measuring window occurs near the Fermi level crossing.

directly related to the Fermi surface [3,5]. Whereas for three-dimensional materials these line features represent cuts through a three-dimensional Fermi surface, the $\mathbf{k}(E)$ method provides the full topology of the Fermi surface for two-dimensional systems like graphite [4] or the quasi-two-dimensional cuprates [6,7].

It is generally believed that at high doping cuprates have a large *hole* Fermi surface centered at (π,π) [1,2]. In a recent paper by Chuang *et al.*, published after the submission of this manuscript, a Fermi surface centered around $(0,0)$ is reported [8]. However, this result is at present controversially discussed. Furthermore, it is also accepted by most groups that the volume of the Fermi surface is shrinking if the doping is reduced [9–12]. The topology of the Fermi surface of underdoped crystals, however, is under debate and controversial interpretations of ARUPS results concerning this point have been published. Dessau *et al.* [9] and Vobornik *et al.* [10] emphasize a transformation from a large Fermi surface centered at (π,π) at optimal doping into a small Fermi surface (so-called hole pockets) located at $(\frac{\pi}{2},\frac{\pi}{2})$ for underdoped samples. Ding *et al.* [11,12] report even for highly underdoped systems a large Luttinger Fermi surface [13] with a volume proportional to $(1+x)$, with x being the hole concentration.

In addition to the volume change a pseudogap opening below a temperature $T^* > T_c$ has been observed with ARUPS in underdoped samples [11]. This pseudogap shows the same symmetry and similar gap sizes as the real superconducting gap below T_c, *i.e.* it opens around $(\pi,0)$ but vanishes around $(\frac{\pi}{2},\frac{\pi}{2})$. As discussed by Marshall *et al.* [14] this might lead to photoemission maps at E_F which indicate "pockets" around $(\frac{\pi}{2},\frac{\pi}{2})$. In a recent ARUPS work Saini *et al.* [15] reported a pseudogap around $(\pi,0)$ also in an optimally doped cuprate, but their results have not yet been confirmed by other photoemission groups.

The Fermi surfaces in [9–12] have all been determined with energy resolutions of some ten meV but only few points in **k**-space have been measured. Our $\mathbf{k}(E)$ ARUPS method allows a complete mapping of more than the first Brillouin zone of these cuprate materials. It is therefore well suited for the study of the influence of doping on the topology and the volume of the Fermi surface. In earlier work we successfully applied this $\mathbf{k}(E)$ method to map the full normal state Fermi surface of $Bi_2Sr_2CaCu_2O_{8+\delta}$ [6,16] and of Pb-$Bi_2Sr_2CaCu_2O_{8+\delta}$ [17] samples which were nearly optimally doped. These results confirmed that large Fermi surfaces around (π,π) exist. The validity of the data interpretation in terms of Fermi surface contours made from $\mathbf{k}(E)$ maps has also been corroborated by measuring the dispersion in series of energy distribution curves (EDC's) and/or the corresponding angular distribution curves (ADC's) [6,16] (see also Fig. 1). In addition to a large Fermi surface additional lines have been observed which are likely to be missed by the standard $E(\mathbf{k})$ method. Some of these additional lines can be attributed to the geometrical superstructure present in Bi2212 crystals [16,18]. A second set of additional lines turned out to be a replica of the large Fermi surface translated by vectors $(0,0)-(\pm\pi,\pm\pi)$. Such *shadow bands* were proposed by Kampf and Schrieffer as being related to antiferromagnetic spin correlations [19,20]. While the existence of the shadow bands has been confirmed by other photoemission measurements [15,21], their origin is under debate. Some groups argue that the shadow bands might be as well of structural origin [22,23]. If the shadow bands observed in an ARUPS experiment are of antiferromagnetic origin, then we would argue that their intensity should increase if the hole concentration is lowered since one gets closer to the antiferromagnetic insulating phase [20]. This aspect is investigated in this work together with the doping dependence of the topology and the volume of the Fermi surface.

2 Experiment

2.1 Samples

Differently doped $Bi_2Sr_2CaCu_2O_{8+\delta}$ (labelled Bi2212) and one (undoped) $Sr_2CuO_2Cl_2$ (SCOC) single crystals have been investigated. SCOC is an antiferromagnetic insulator, which is generally taken as a representative of undoped cuprates. All samples were grown from non-stoichiometric systems which consist of solute and flux,

forming a high-temperature solution [24]. The resulting single crystals used for the photoemission experiments are *c*-axis oriented platelets with an area of about 2×2 mm^2 and a thickness of 0.1 mm. The superconducting transition temperatures T_c were determined by resistivity measurements using a four-point contact method on the same crystals which were used for the photoemission experiments. One set of samples was, according to the experimental T_c *versus* hole concentration curve of Groen *et al.* [25], in the vicinity of optimal doping and had a T_c of 84 K. We label these samples Bi2212(OPT). Overdoped samples (Bi2212(OD)) were produced by annealing Bi2212 in a 4 kbar oxygen atmosphere [26], having a T_c of 60 K. Underdoped samples (Pr-Bi2212(UD)) were prepared by adding 5% of Pr. X-ray photoelectron diffraction measurements show that at least in the near-surface region Pr occupies Ca sites [27]. The T_c of Pr-Bi2212(UD) is 30 K. The corresponding hole concentrations are $x = 0.07$ for Pr-Bi2212(UD), $x = 0.185$ for Bi2212(OPT) and $x = 0.265$ for Bi2212(OD). These values have been extracted from an experimental T_c *versus* hole concentration curve [25].

For the photoemission experiments the single crystal platelets were fixed onto Cu sample holders using Ag epoxy glue [28]. Clean surfaces were obtained by cleaving the crystals in ultra-high vacuum at room temperature using an ordinary adhesion tape. During this procedure, the pressure remained below 2×10^{-10} mbar. The cleaved part sticking on the adhesive tape was removed *via* the fast entry lock of the vacuum system. Every cleaved surface is unique and a different number of defects will be present. We assume that if the amount of defects is too high the crystallinity and/or the oxygen content in the surface region will be seriously modified. This could be the reason why approximately one third of the cleaves show no anisotropy in $\mathbf{k}(E_F)$ measurements. In contrast to what one would expect at least for optimally and overdoped samples we were unable to observe a pronounced leading edge at the Fermi level in these cases in the ultraviolet photoelectron spectrum.

The crystallinity of the cleaved surfaces was checked by low energy electron diffraction (LEED). For all pure and Pr-doped Bi2212 sample surfaces the geometrical "5×1" superstructure described in [18] was observed. The modulation period and the a_0 and b_0 lattice constants agree within 5% with the values found for bulk material (modulation period 4.8, lattice constants 5.396 Å and 5.397 Å, respectively [18]). However, it is not possible to make a statement about the modulation amplitudes. For SCOC we observed sharp LEED patterns, which showed a (1×1) symmetry with respect to the two-dimensional Cu-Cu nearest-neighbor unit cell. The Cu-O plane lattice constant of SCOC at the surface is in agreement with the bulk value of 3.97 Å [29].

2.2 Photoemission

The photoemission experiments were performed in a modified VG ESCALAB 220 spectrometer with a base pressure of 6×10^{-11} mbar. The spectrometer is equipped with a fast entry lock system which allows to introduce samples without breaking the vacuum. The core of the experimental setup is a custom made two-axis sample goniometer. This goniometer allows a computer-controlled rotation of the sample in polar and in azimuthal direction with an accuracy of better than 0.2°. The photoelectrons are detected in a standard 150 mm hemispherical analyzer with 6 channeltron electron counters. Two iris-apertures allow an adjustment of the spatial and angular resolution. The ultimate angular resolution is better than 1° full width at half maximum (FWHM), as measured using the surface state of an Ag(111) surface. All experiments presented here have been performed at 300 K (for Bi2212) or at 330 K (to suppress charging effects in SCOC). The energy resolution is set to 100 meV which corresponds to the k_BT broadening of a Fermi-Dirac distribution at 300 K. The angular resolution was set to be 7° FWHM. The UV radiation for the ARUPS experiments is produced in a helium electron cyclotron resonance (ECR) plasma (Gammadata VUV 5 000 He discharge lamp) which is excited by 10 GHz microwave radiation. The produced UV line spectrum is then monochromatized by a toroidal grating. All ARUPS results presented in this paper have been measured with the He Iα line with a photon energy of 21.22 eV. Using this photon energy it follows from the relation $k_{\|}(\text{Å}^{-1}) = 0.51\sqrt{(h\nu - \phi)(\text{eV})}$ for the **k**-vector of the photoelectron in vacuum [7,30], that for photoelectron emission from the Fermi level a circular area with a radius of (2.14 ± 0.01) Å^{-1} in reciprocal space can be probed. We assumed for the work function ϕ a value of (3.6 ± 0.1) eV. This is an average value obtained by measuring the photoemission low-energy cut off from different cleaves on different Bi2212 crystals. Even though the measured work function of our samples may appear low, it is this value which has to be taken for a correct scaling of $k_{\|}$-maps. One should note that the work function depends among other factors also on the roughness of a surface and this quantity is certainly different between different samples. For He Iα radiation the monochromator reduces the contribution of higher energy He radiation to less than 0.2%. This allows to deduce all information from the raw data sets. The He partial pressure during operation reaches in the main chamber 2×10^{-8} mbar. A detailed description of the UV lamp and monochromator set-up is given in [31].

As an experimental constraint the problem of sample aging has to be addressed. At room temperature the Bi-O surface layer [32,33] of cleaved Bi2212 is rather inert to residual gases in the UHV chamber at pressures below 5×10^{-10} mbar. However, we have observed sample modifications under the influence of high-flux UV radiation. The position of the leading edge in an UPS spectrum is shifting towards higher binding energies and the shape of the spectrum around E_F changes. The shift rate with He Iα radiation (flux: 5.6×10^{11} photons/s mm^2) is approximately 3 meV/h. A careful analysis of this effect leads to the conclusion that UV light is underdoping the surface region of Bi2212 samples [34]. The doping decreases exponentially with photon exposure which limits the data acquisition time. All Fermi surface experiments shown here

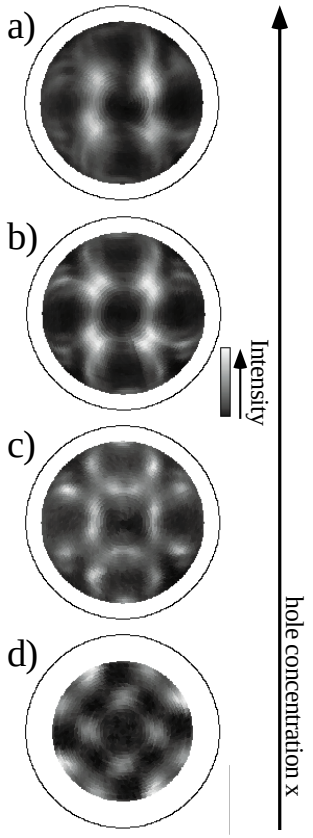

Fig. 2. He Iα (21.22 eV) excited $k_\parallel$ maps of differently doped cuprates plotted linear in $k_\parallel$ (see text). (a) overdoped Bi2212(OD); (b) optimally doped Bi2212(OPT); (c) underdoped Pr-Bi2212(UD); (d) insulating $Sr_2CuO_2Cl_2$. The Fermi surface maps (a-c) show raw data and have been measured at 300 K. For each Fermi surface the photoelectron intensity has been measured at 3284 different points in **k**-space. The $k_\parallel$ map of the valence band maximum of SCOC has been measured at 2254 different points and is four-fold averaged. This experiment has been done at 330 K and the valence band maximum was located at 0.9 eV binding energy.

are therefore performed in such a way that the shape of a normal emission spectrum measured after cleaving and after a Fermi surface measurement remains unchanged. The observed shift of the leading edge is less than 10 meV in all cases. On the other hand the doping change induced by the UV light offers the unique possibility to study different doping levels on the *same* cleaved surface. Here this effect is exploited to study the doping-dependence of the shadow bands.

3 Topology and volume of the Fermi surface

3.1 $k_\parallel$-maps

Figure 2 shows room temperature $k_\parallel$-maps for four different hole concentrations measured with monochromatized He Iα photons. The center point of each pattern represents normal photoelectron emission ($k_\parallel = 0$), the outer circle emission along the crystal surface ($k_\parallel = 2.14$ Å^{-1} for Bi2212, $k_\parallel = 1.92$ Å^{-1} for SCOC). The maps shown in Figure 2 are plotted in a linear $k_\parallel$ scale and all photoelectron intensities are displayed in a linear grey scale with high intensity given in white. Except for a four-fold averaging of the valence band maximum map of SCOC (Fig. 2d) all data shown are raw data without any additional treatment. For SCOC this averaging has been necessary because due to inhomogeneities of the cleaved surface the valence band maximum features were not observed in every quadrant of the intensity map. Nonetheless the existence of such features around $(\frac{\pi}{2}, \frac{\pi}{2})$ can be deduced unmistakably from the raw data.

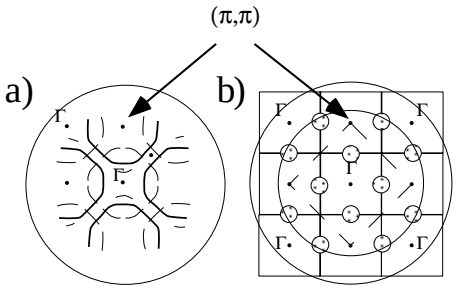

Fig. 3. (a) Guide to the eye for the Fermi surface map of Bi2212(OPT) (see Fig. 2b). The thick lines indicate the large Fermi surface. (b) Guide to the eye for the valence band maximum map shown in Figure 2d. The dashed square shows the structural Brillouin zone, the solid squares the antiferromagnetic zone boundaries.

One may raise the question whether it is actually possible to obtain reasonable results with resolutions of 100 meV and 7° FWHM. Our results on near-optimally doped samples (see also Ref. [6]) reveal very similar Fermi surface contours as do measurements performed in the $E(\mathbf{k})$ mode and with better resolution (see *e.g.* Refs. [1,21]). Ronning *et al.* extract the Fermi surface location using spectra similar to the ones we show in Figure 1 [35]. This gives us confidence that our measurements are well suited to study the evolution of Fermi surface contours. It is of course not possible to be conclusive on intensities but the reader should note that the analysis of the Fermi surface volume as a function of the hole concentration which is presented in the next section is based exclusively on the shape of the Fermi surface.

First the Fermi surface map of Bi2212(OPT) shown in Figure 2b will be discussed. A guide to the eye for this measurement is shown in Figure 3a. Clearly a large Fermi surface centered at (π, π) (solid lines in Fig. 3a) can be observed at this doping level. Taking the position of the $(\pi, 0)$ point at $k_\parallel = 0.82$ Å^{-1}, the measured work function ϕ and the relation $k_\parallel(\text{Å}^{-1}) = 0.51\sqrt{(h\nu - \phi)(\text{eV})}\sin\theta$ a polar emission angle $\theta = 22.5°$ off normal is found for the $(\pi, 0)$ point. This corresponds to the emission angle of the $(\pi, 0)$ point as extracted from the $k_\parallel$ map. The additional weak lines (dashed lines in Fig. 3a), representing the *shadow bands* are discussed in Section 4. The small features (*e.g.* the line between the Γ-point and the large Fermi surface) are related to the geometrical superstructure (see Fig. 8a and [6,16] for details). We would like

to emphasize that the photoelectron intensity is quite high around the $(\pi, 0)$ points and that relatively weak intensity is found along the $(0,0) - (\pi,\pi)$ line. Similar observations can be made in the Fermi surface map of overdoped Bi2212(OD), as shown in Figure 2a.

The volume of the hole Fermi surface is defined as the area of one hole barrel centered at (π, π). This volume is smaller for Bi2212(OPT) compared to Bi2212(OD) (see Sect. 3.2 for a quantification of this statement). This is consistent with the reduced number of holes per Cu atom in Bi2212(OPT). For strongly underdoped Pr-Bi2212(UD) (Fig. 2c) contours of a Fermi surface centered at (π, π) are still perceptible. Again consistent with the further decreased number of holes/Cu the Fermi surface volume is smaller than for Bi2212(OPT). However, there are significant differences between the Fermi surface map of Pr-Bi2212(UD) with respect to the Fermi surfaces of Bi2212(OPT) and Bi2212(OD). Compared to the measurements of Bi2212(OD) and Bi2212(OPT) we find a strongly reduced relative intensity in the $(\pi, 0)$ region. This may be explained by the fact that the van Hove singularity which is about 50 meV below E_F for high doping moves farther away from E_F if the hole concentration is lowered. The high intensity around $(\pi, 0)$ for Bi2212(OD) and Bi2212(OPT) may therefore be partially due to contributions from the van Hove singularity, intensity which would then be missing for Pr-Bi2212(UD). The shift of the relative intensities from $(\pi, 0)$ to $(\frac{\pi}{2}, \frac{\pi}{2})$ in Pr-Bi2212(UD) could also be interpreted as an indication for the opening of a pseudogap around $(\pi, 0)$, as reported by Ding *et al.* [11] although our measuring window is larger than the reported gap. For an underdoped sample with T_c=10 K they found a lower limit for T^* of 300 K. Therefore it could be possible that in the Pr-Bi2212(UD) sample with a T_c of 30 K effects of the pseudogap are observed at 300 K, the sample temperature during our experiments. Due to the experimental resolution of 100 meV, thermal broadening effects and since no temperature-dependent measurements have been done so far, we cannot be conclusive. Furthermore, the presence of flat bands near E_F around $(\pi, 0)$ (attributed to the van Hove singularity) might influence the spectral weight measured in the experiment. An alternative view of the $k_\parallel$ map of Pr-Bi2212(UD) is that it is a precursor of the formation of hole pockets around $(\frac{\pi}{2}, \frac{\pi}{2})$. Such a transformation of a large Fermi surface centered at (π, π) for high doping into pockets around $(\frac{\pi}{2}, \frac{\pi}{2})$ in the underdoped regime is supported by the position of the valence band maximum of the undoped material which is also located at $(\frac{\pi}{2}, \frac{\pi}{2})$. This is shown in Figure 2d and in the corresponding guide to eye (Fig. 3b). A more detailed and quantitative description of the dispersion of the uppermost valence band of SCOC will be given in Section 5.

An interesting feature which however we cannot explain at present is the intensity dip on the Fermi surface contour near $(\frac{\pi}{2}, \frac{\pi}{2})$. The dip is observable on all three samples and it is probably not related to our specific samples or our experiment, because other groups have made the same observation [15]. Such intensity variations may be related to matrix element effects, as discussed in a recent publication by Bansil and Lindroos [36]. Due to our limited energy resolution we are not able to make further comments concerning the intensities of the $k_\parallel$-maps. As mentioned above, a change of the Fermi surface topology, *i.e.* a transformation from a large Fermi surface into hole pockets is consistent with our data. We will show in the following section, that an analysis of the Fermi surface volume as a function of the hole concentration gives evidence for a change in the Fermi surface topology at low doping levels.

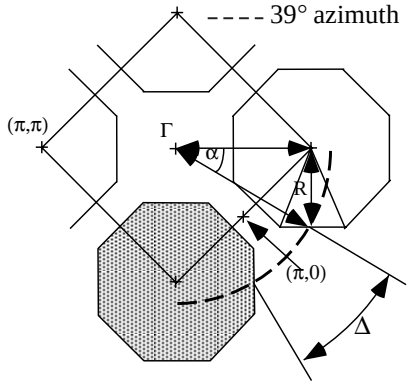

Fig. 4. Approximation of the Fermi surface by regular octagons. The solid square represents the Brillouin zone, the dashed circle segment the location of the 39° azimuthal cut. The Fermi surface intersection angle Δ is used as a measure for the Fermi surface volume.

3.2 Evolution of the Fermi surface volume with doping

The Fermi surface volume is equal to the area of one single Fermi surface barrel around (π, π) (see Fig. 4). Taking a half filled band at zero doping and assuming a Fermi surface topology which does not change with the doping x, then the Fermi surface volume should scale as $(1 + x)$ according to Luttingers theorem [13]. To determine the Fermi surface volume, azimuthal scans at a particular polar angle have been measured. We have arbitrarily selected a polar angle of 39° (see Fig. 4). The angular distance between two pieces of the Fermi surface on this scan is labelled Δ. Obviously, the larger Δ, the smaller is the volume of the hole Fermi surface. Such azimuthal scans have been measured for all three differently doped Bi2212 samples (see Fig. 5). For all three samples peaks originating from the Fermi surface (labelled FS) are clearly visible and thus, Δ can be determined accurately. The reader should notice that effects of the pseudogap, if they were present in Pr-Bi2212(UD) at 300 K, should not be seen in this region of **k**-space. The additional peaks (SB) are the shadow band peaks, which are discussed in Section 4. The detected Δ-values are $\Delta = (22° \pm 1°)$ for Bi2212(OD), $\Delta = (24° \pm 1°)$ for Bi2212(OPT), and $\Delta = (31° \pm 2°)$ for Pr-Bi2212(UD), respectively. Each value is the average of four possible Δ values obtained from a 360° azimuthal scan. The positions of the Fermi surface locations were determined by Gaussian fits. From the values of Δ

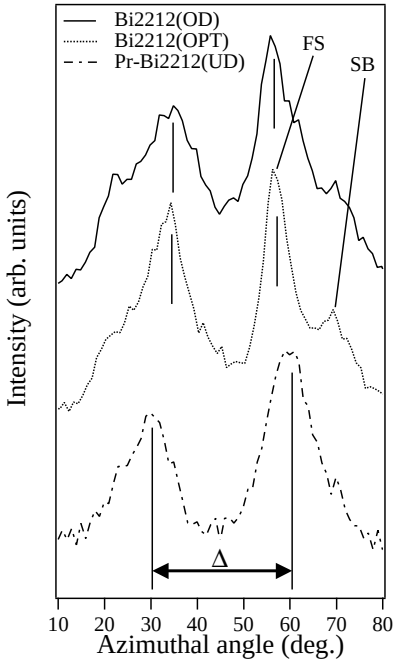

Fig. 5. Extract of the $\theta = 39°$ azimuthal scan of Bi2212(OD), Bi2212(OPT) and Pr-Bi2212(UD) measured at E_F. The vertical lines indicate how Δ is measured. FS labels the large Fermi surface crossings, SB the shadow bands.

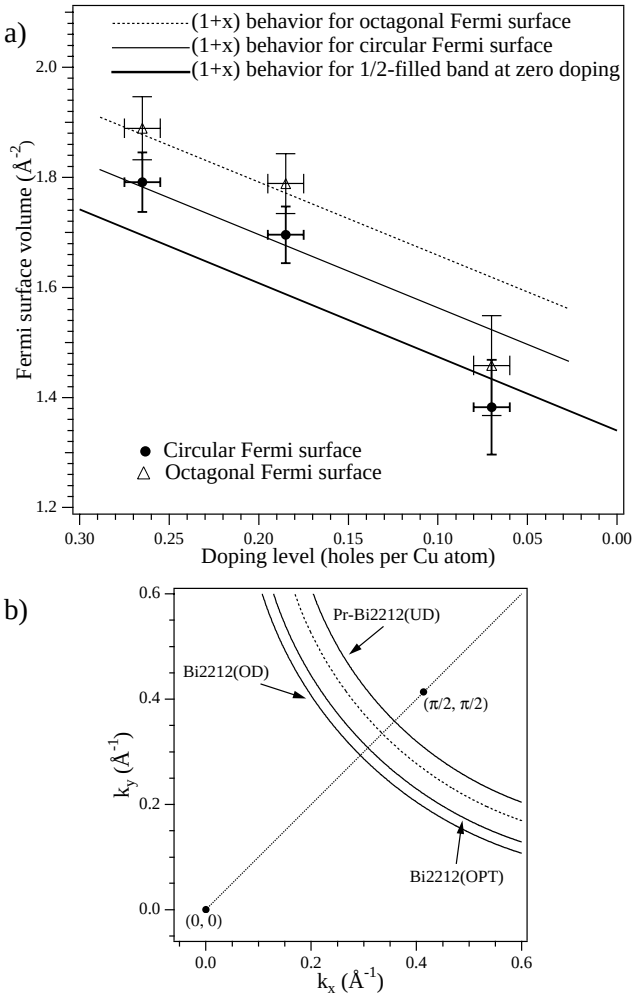

Fig. 6. (a) Fermi surface volumes as a function of the hole concentration for circular (filled circles) and octagonal (empty triangles) Fermi surface shapes. The straight lines indicate the Fermi surface volume evolution for a Luttinger Fermi surface. (b) Fermi surfaces of Bi2212(OD), Bi2212(OPT) and Pr-Bi2212(UD) in the $(\frac{\pi}{2}, \frac{\pi}{2})$ region assuming a circular Fermi surface shape. The dashed circle segment indicates the Luttinger Fermi surface for a doping level corresponding to the Pr-Bi2212(UD) sample.

the volume of the Fermi surface has been calculated within a simple model: The shape of one hole barrel around (π, π) is approximated by a regular octagon (see Fig. 4). Furthermore, it is assumed that the shape of the Fermi surface is invariant upon doping as it is suggested from the $k_\parallel$ maps shown in Figure 2. From Figure 4 it follows that the angle α is equal to $45° - \frac{\Delta}{2}$, and from the distance between Γ and (π, π) and the radius of the 39° azimuth, the area of the octagon is determined. The error of ± 0.1 eV for the work function Φ has been considered for calculating the **k**-space circle covered by the 39° azimuth. To check how sensitive the Fermi surface volume calculated with this model is to the assumed shape of the Fermi surface, the volume analysis has also been done for a circular Fermi surface with radius R (see Fig. 4), still centered at (π, π). The Fermi surface volumes for the different hole concentrations x are shown in Figure 6a. The hole concentrations x have been determined from an experimental T_c *versus* hole concentration curve [25]. Note that the determination of the hole concentration in [25] has not been done on the same Bi2212 samples as used for our photoemission experiments. Therefore an error of ± 0.01 was assumed for the hole concentration x. Because in the T_c region of Pr-Bi2212(UD) and Bi2212(OD) the T_c *versus* hole concentration curve is very steep and T_c can be accurately determined, this error value is reasonable. For Bi2212(OPT) the x-value corresponding to the maximal T_c has been taken. The straight lines in Figure 6a indicate the gradient of the Fermi surface volume assuming a $(1 + x)$ behavior. The thick solid line is obtained by taking the half filled band at zero doping. The Fermi surface volume is in this case 1.34 Å^{-2}, *i.e.* half the area of the two-dimensional Brillouin zone. One finds that the Fermi surface volumes of Bi2212(OD) ($x = 0.265$) and Bi2212(OPT) ($x = 0.185$) scale almost perfectly with a $(1+x)$ gradient. This is valid for both, circular (filled circles, thin solid line) and octagonal (empty triangles, thin dashed line) Fermi surface shapes. For Pr-Bi2212(UD) ($x = 0.07$), however, we find for both shapes a significant deviation from the $(1+x)$ gradient. It appears that the Fermi surface of Pr-Bi2212(UD) ($T_c = 30$ K, $x = 0.07$) may not fit into Luttingers theorem. This is also illustrated in Figure 6b: circular Fermi surfaces for different hole concentrations are drawn in the $(\frac{\pi}{2}, \frac{\pi}{2})$ region. The radii R have been determined as described above using Δ. The solid segments represent the Fermi surfaces

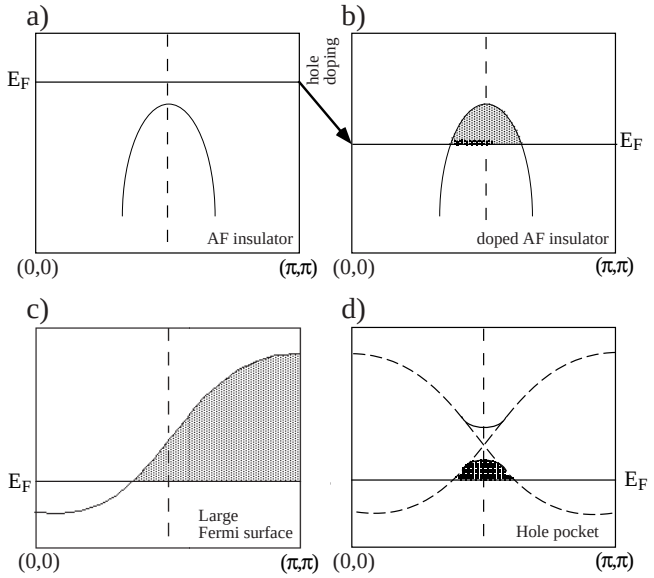

Fig. 7. Suggested cuprate bandstructure at different doping levels. The filled areas indicate hole states. (a) Valence band maximum at $(\frac{\pi}{2}, \frac{\pi}{2})$ for the antiferromagnetic insulator. (b) Hole doping shifts the Fermi level into the valence band. (c) Large Fermi surface as observed in highly doped samples. (d) A reduced Brillouin zone transforms a large Fermi surface into hole pockets at $(\frac{\pi}{2}, \frac{\pi}{2})$.

of Bi2212(OD), Bi2212(OPT) and Pr-Bi2212(UD) as circles centered at (π, π). The dashed circle segment shows the Fermi surface for a hole concentration of $x = 0.07$ (Pr-Bi2212(UD)) if the Fermi surface volume would scale with $(1 + x)$ which is obviously not the case.

Our experiments therefore do not confirm the results obtained by Ding *et al.* [11,12] who found even for a strongly underdoped sample with a T_c of 15 K a Fermi surface volume which is in agreement with a $(1 + x)$ gradient.

3.3 Discussion

We discuss in this section what may be the consequences of a deviation from Luttingers theorem for the strongly underdoped sample. For us, a change of the Fermi surface topology is possible. As mentioned, it cannot be ruled out that we see effects of a pseudogap in Pr-Bi2212(UD) at 300 K. However, as confirmed by Ding *et al.* [12], the minimum gap locus in the pseudogap regime coincides with the Fermi surface in the gapless regime. The authors [12] find that the $(1 + x)$ relation remains valid in this case. A simple interaction-induced formation of preformed pairs above T_c, as implied by Trivedi *et al.* [37] would not cause a deviation from $(1 + x)$, in contrast to our observations.

Since we have an indication for a non-Luttinger-like behavior in Pr-Bi2212(UD), other possible explanations have to be considered, such as a topological modification of the Fermi surface. Figure 7 illustrates such a transformation, relating two experimentally established points, the existence of large Luttinger Fermi surfaces centered at (π, π) for high doping (Fig. 7c) and the position of the valence band maximum around $(\frac{\pi}{2}, \frac{\pi}{2})$ for zero doping (Fig. 7a). The dispersion of this highest occupied band strongly suggests that upon doping the Fermi level drops into the valence band [38] and hole-pockets around $(\frac{\pi}{2}, \frac{\pi}{2})$ are formed (Fig. 7b). Figure 7d illustrates how this topology change may be induced: If the Brillouin zone is reduced such that the zone boundary moves from (π, π) to $(\frac{\pi}{2}, \frac{\pi}{2})$, then a second band will appear. This band and the band forming a large Fermi surface will split up and a hole pocket at $(\frac{\pi}{2}, \frac{\pi}{2})$ develops. This new symmetry corresponds to the symmetry of antiferromagnetically ordered spins within the copper oxide planes [6]. The idea that spin fluctuations play an important role in the electronic structure is widely disseminated in theoretical models [19,20,39–42], and it is fostered by a simple argument: Undoped cuprates are antiferromagnetic insulators and short range spin fluctuations persist up to high doping levels [43,44].

4 Doping-dependence of shadow bands

In this section the doping-dependence of the shadow band features observed on the Fermi surface of Bi2212 [6] are discussed. The shadow bands (SB) are a replica of the large Fermi surface (LFS) translated by vectors $\pm(\pi, \pi)$. This is illustrated in Figure 8a: The LFS is drawn with thick solid lines. For simplification we again use regular octagons to represent the Fermi surface barrels. The SB are represented with thick dashed lines.

As mentioned in the introduction a possible origin for the shadow bands are antiferromagnetic spin fluctuations [19,20], but as discussed in [45] a structural origin cannot be ruled out. In principle the situation should be clarified if the doping-dependence of the shadow band intensity is investigated.

As an additional complication one has to consider the effects of the geometrical "5×1" superstructure. However we do not observe 5 copies of the LFS but just the two which are displaced by roughly $\pm 0.2(\pi, \pi)$ (dashed thin lines in Fig. 8a). This is in agreement with previous work [6,16]. As a consequence of the modulation-related features in some regions of the **k**-space SB and modulation-related features are superimposed. The solid circle in Figure 8a indicates the location of a 39° off normal azimuth. For the regions labelled A, D, E and H, there is no overlap between SB and modulation features on this specific azimuth. For the regions B, C, F and G, however, one finds that SB and modulation features are superimposed. The SB features in B, C, F and G are therefore certainly influenced by the geometrical structure.

Figure 8b shows an azimuthal intensity scan through the Fermi surface of Bi2212(OPT) measured at a polar emission angle of 39° off normal. The vertical arrows indicate the positions of the LFS peaks. An important point is that due to the geometrical superstructure the scan reveals an approximate two-fold symmetry which makes features B, C, F and G much more pronounced. There SB and modulation-related bands are superimposed (Fig. 8).

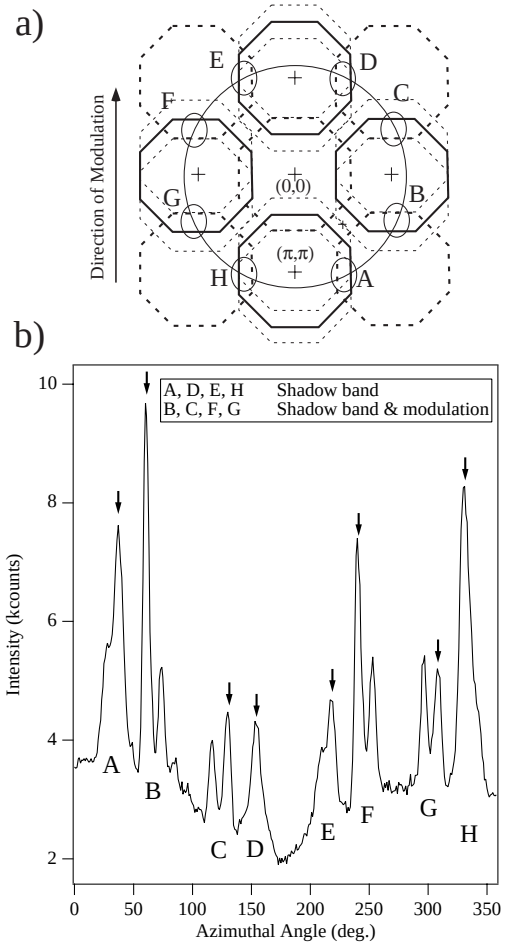

Fig. 8. (a) Sketch of the reciprocal space for Bi2212(OPT). The Fermi surface barrels are drawn as regular octagons. Thick solid lines indicate the large Fermi surface, thick dashed lines the shadow bands and thin dashed lines modulation related replicas. The circle indicates the $\theta = 39°$ azimuth. The labels A to G are discussed in the text. (b) Azimuthal cut through the Fermi surface of Bi2212(OPT) at $\theta = 39°$. Intensity variations are discussed in the text.

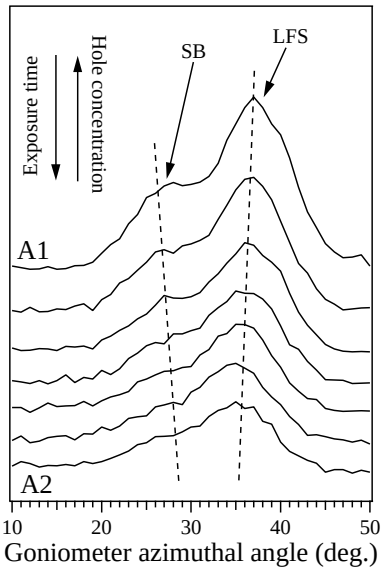

Fig. 9. Evolution of large Fermi surface bands and shadow bands with decreasing doping level. Different curves have been measured at identical angular settings (showing region A of Fig. 8) but with increasing exposure time to UV radiation. The dashed lines indicate the angular position of the large Fermi surface band and the shadow band.

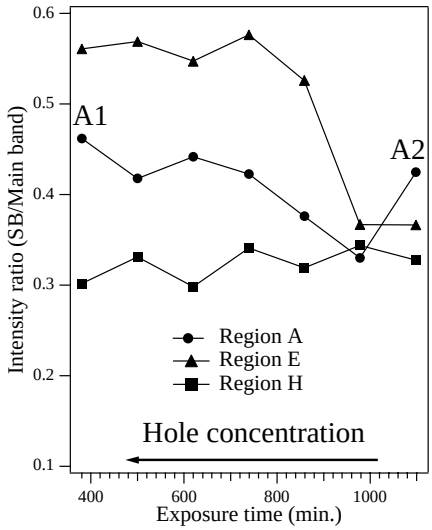

Fig. 10. Intensity ratio between shadow band and large Fermi surface peaks calculated from the data shown in Figure 9 (region A) and for the regions E and H.

As a consequence, clear additional peaks are observed in contrast to the regions A, D, E and H, where the "pure" SB just appear as shoulders of the LFS peaks.

There are several reasons for the intensity variations of large Fermi surface and shadow band peaks in the different quadrants of the scan: There is a slight misalignment of the sample surface due to the fixation process with the Ag epoxy (at most 2°). The crystal c-axis is therefore not parallel to the azimuthal rotation axis, and the scan covers a certain spread of polar angles with respect to the c-axis. A second point is, that, while rotating the crystal, the sample region from which photoelectrons are detected slightly varies. If the surface after cleaving of the crystal is somewhat inhomogeneous, intensity variations can result. This fact has the consequence that relative shadow band intensities from different samples are difficult to compare.

In order to study the trend in intensity ratios between different transitions as a function of hole doping we therefore performed an experiment where systematic differences between samples are minimized: The hole concentration is varied by in situ photodesorption of oxygen from the samples [34]. This photodesorption process is not fully understood yet. It is not clear from which layers the O atoms are ejected but it is likely that their origin are predominantly the Bi-O surface layer or the underlying Sr-O layer. It cannot be ruled out that also O atoms from the Cu-O layers are ejected. However photoemission experiments reveal similar results for UV irradiated samples and for underdoped Pr-Bi2212(UD) [34]. Furthermore

we know from LEED experiments that the structure within the near-surface region remains unchanged. This "photoinduced underdoping" allows to study different doping levels on the same cleaved surface. Furthermore we took advantage of the possibility that the sample goniometer allows endless azimuthal rotations. During such a measurement the surface is continuously exposed to UV radiation and correspondingly the doping level continuously decreases [34]. Figure 9 shows a 40° window from such a multiple azimuthal scan showing always the LFS peak and the SB-shoulder of region A (as defined in Fig. 8), *i.e.*, always the same region of the Brillouin zone measured on the same part of the sample. Intensity variations can therefore be directly related to changes in the doping level. The only difference between the scans shown in Figure 9 is the exposure time to the UV radiation and thus the hole concentration. The top spectrum of Figure 9 (labelled *A1*) is measured on a freshly cleaved Bi2212(OPT) sample. The hole concentration is therefore assumed to be 0.185 holes per Cu atom. The last spectrum (*A2*) is measured after an UV exposure time of about 16 hours. The corresponding hole concentration is close to the value of Pr-Bi2212(UD) which is 0.07 holes per Cu atom. The dashed lines in Figure 9 indicate the positions of large Fermi surface band and shadow band as obtained by Gaussian fits. The decrease in angular splitting indicates a shrinking of the Fermi surface upon UV exposure. This is a clear indication that the doping level has been lowered.

To determine the relative shadow band intensity a linear background was subtracted from each angular cut shown in Figure 9. LFS and SB peaks were then fitted by Gaussians. The widths of the LFS band and the SB were identical but could vary for each curve shown in Figure 9. The ratio of SB-intensity and LFS band intensity resulting from this procedure at this specific location in **k**-space (region A) is shown in Figure 10, together with analogous values obtained at regions E and H. In region D the SB is extremely weak so that no reliable curve fit could be obtained.

In contrast to what one would expect for underdoping and assuming an antiferromagnetic origin of the SB, no increase of the shadow band intensity is observed. The slight trend of decreasing shadow band intensity with decreasing hole concentration may be of structural origin. However, the reader should note that the present result does not rule out that antiferromagnetic correlations may play an important role in the evolution of the Fermi surface in the underdoped regime as has been sketched in Section 3.

5 The uppermost valence band of SCOC

In Figure 2d a complete $k_{||}$ map measured at the valence band maximum of undoped $Sr_2CuO_2Cl_2$ (SCOC) is presented. In order to corroborate that the intensity features observed in Figure 2d actually correspond to the apex of the uppermost band of SCOC we will present in the following more detailed ARUPS results obtained from this compound.

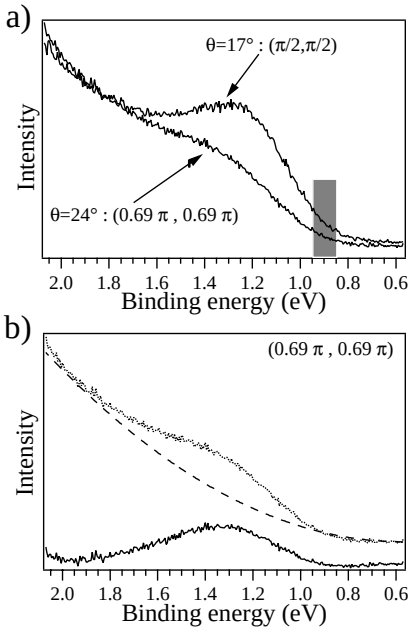

Fig. 11. (a) Energy distribution curves from SCOC measured at $(\frac{\pi}{2}, \frac{\pi}{2})$ (polar angle 17°) and at $(0.69\pi, 0.69\pi)$ (24°). The grey bar indicates the measuring window for the $\mathbf{k}_{||}$-map shown in Figure 2d; (b) Illustration of the quadratic background subtraction procedure. From the raw data (dots) a quadratic background (dashed line) is subtracted. The result is a peak (solid line).

A problem in ARUPS experiments with insulators is that one has to deal with sample charging. We find that the charging is constant for all photoelectron emission angles at a given temperature. Slightly heating the crystal reduces the charging and a saturation of the charge compensation occurs at about 330 K.

As in Bi2212 we also observed an aging effect in SCOC due to the UV radiation. Interestingly, the aging seems to be weaker at elevated temperatures [27]. In all experiments with SCOC the photon flux was reduced and the measurement time on one specific cleave was limited to about one hour to have stable sample conditions. As a last experimental aspect we have to stress that the energy position of the valence band maximum varies from cleave to cleave. In our samples the valence band maximum is found within a binding energy range between 1.0 and 1.7 eV. The reason for this is probably given by a different pinning of the Fermi level within the insulator gap due to a varying number of defects at the surface [46].

For the measurement presented in Figure 2d the electron analyzer energy has been fixed at a binding energy of 0.9 eV. By this choice we are sure to measure features which are related to the valence band maximum. In order to obtain quantitative information on the band dispersion near the valence band maximum a series of energy spectra along the $(\pi, \pi) - (0, 0)$ and along the $(\pi, 0) - (0, 0)$ directions have been measured. Figure 11a shows two energy distribution curves along the $(\pi, \pi) - (0, 0)$ direction. The spectrum measured at a polar angle of 17°

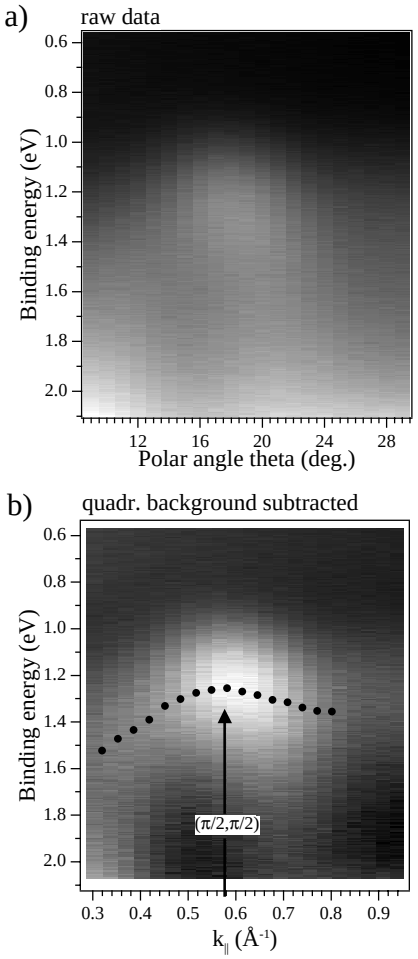

Fig. 12. He I excited energy distribution curves of SCOC for a continuous range of polar angles along the $(\pi,\pi)-(0,0)$ direction. Photoemission intensities are plotted in a linear grey scale. Raw data are shown in a), in b) a quadratic background has been subtracted. The black dots indicate the peak position as determined by a Gaussian fit (see text).

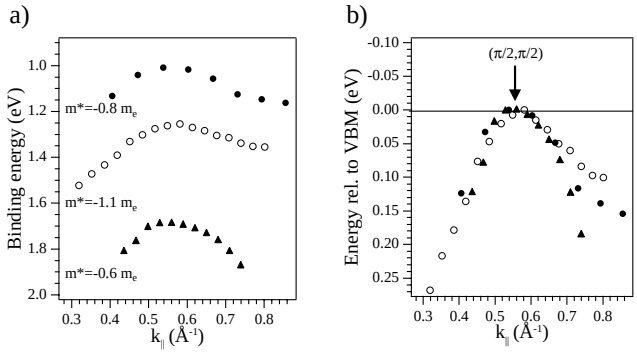

Fig. 13. (a) Dispersion of the uppermost valence band of SCOC along the $(\pi,\pi)-(0,0)$ direction for different cleaves. In (b) these scans are normalized to the valence band maximum (VBM).

off normal corresponds to $(\frac{\pi}{2},\frac{\pi}{2})$ and shows a peak at the valence band maximum which is centered at 1.26 eV binding energy for this specific cleave. In the spectrum measured at a polar angle $\theta = 24°$ $(0.69\pi, 0.69\pi)$ the peak is much weaker and is located at higher binding energy. This behavior is very similar to that of spectra near a Fermi level crossing in optimally doped Bi2212. This suggests that hole doping is moving the Fermi level into the valence band of the antiferromagnetic insulator [38]. To determine the exact peak positions a quadratic background has been subtracted from each spectrum around $(\frac{\pi}{2},\frac{\pi}{2})$. This is illustrated in Figure 11b. The background subtraction yields a curve with a well-defined peak. Its position can be determined accurately by a Gaussian fit. This procedure has been applied to the data described below. Figure 12 shows a series of energy distribution curves measured along the $(\pi,\pi)-(0,0)$ direction. A spectrum has been measured every 1° and all spectra are then combined to a two-dimensional plot with intensities represented in a linear grey scale. Figure 12a shows the raw data. The background subtraction described above significantly enhances the dispersing features (Fig. 12b). The black dots in Figure 12b mark the peak positions as determined by Gaussian fits. This clearly confirms the maxima at $(\frac{\pi}{2},\frac{\pi}{2})$ as observed by Wells *et al.* [38], Pothuizen *et al.* [47] and LaRosa *et al.* [48]. Around $(\frac{\pi}{2},\frac{\pi}{2})$ the peak dispersion can be fitted quite accurately using a parabola, and one obtains the effective mass m^*. We find on this specific cleave a value of $(-1.1\pm0.1)m_e$ for m^*, m_e being the electron mass. This result is in reasonable agreement with the experiment of Wells *et al.* [38] who found a value of (-1.5 ± 0.75) for m^*. Note that the error given in our measurement is extracted from one single scan only. Figure 13a shows the dispersion of the uppermost valence band along the $(\pi,\pi)-(0,0)$ direction for different cleaves. The sample temperature has been in the saturation region of the charge compensation, and the dispersion has been determined in the same way as described above. One can see that the Fermi level is pinned at different locations within the gap for the three measurements. The values of m^* vary between -0.6 and -1.1 m_e. In Figure 13b the three curves are normalized to the valence band maximum energy. Despite the different absolute energy positions of the valence band maxima, it is clearly seen that the dispersion around $(\frac{\pi}{2},\frac{\pi}{2})$ is almost identical for all scans. Therefore, the existence of isolated maxima around $(\frac{\pi}{2},\frac{\pi}{2})$ in the uppermost valence band is confirmed. The effective mass and the binding energy of the valence band maximum, however, can vary from cleave to cleave.

6 Summary

We have demonstrated that angle-resolved ultraviolet photoelectron spectroscopy in the $\mathbf{k}(E)$ mode allows to obtain information about the doping-dependent electronic structure of cuprates in a direct way. Our measurements on differently doped Bi2212 samples confirm large Luttinger Fermi surfaces centered at (π,π) for optimally and overdoped samples. In the strongly underdoped regime

an analysis of the Fermi surface volume yields a deviation from a Luttinger-like behavior which could imply a topological change of the Fermi surface. The valence band maximum in undoped cuprates which is located at $(\frac{\pi}{2}, \frac{\pi}{2})$ and equivalent points makes it likely that the Luttinger Fermi surface at high doping is transformed into small hole-pockets at $(\frac{\pi}{2}, \frac{\pi}{2})$. A possible origin for such a transformation are antiferromagnetic spin correlations even though the shadow bands on the Fermi surface of Bi2212, which are of possible antiferromagnetic origin, do not show an increased intensity in the underdoped regime, *i.e.* closer to the antiferromagnetic insulator.

References

1. Z.-X. Shen, W.E. Spicer, D.M. King, D.S. Dessau, B.O. Wells, Science **267**, 343 (1995).
2. Z.-X. Shen, D.S. Dessau, Phys. Rep. **253**, 1 (1995).
3. T. Straub, R. Claessen, P. Steiner, S. Hüfner, V. Eyert, K. Friemelt, E. Bucher, Phys. Rev. B **55**, 13473 (1997).
4. A. Santoni, L.J. Terminello, F.J. Himpsel, T. Takahashi, Appl. Phys. A **52**, 229 (1991).
5. P. Aebi, J. Osterwalder, R. Fasel, D. Naumović, L. Schlapbach, Surf. Sci. **307**, 917 (1994).
6. P. Aebi, J. Osterwalder, P. Schwaller, L. Schlapbach, M. Shimoda, T. Mochiku, K. Kadowaki, Phys. Rev. Lett. **72**, 2757 (1994).
7. J. Osterwalder, Surf. Rev. Lett. **2**, 391 (1997).
8. Y.-D. Chuang, A.D. Gromko, D.S. Dessau, Y. Aiura, Y. Yamaguchi, K. Oka, A.J. Arko, J. Joyce, H. Eisaki, S.I. Uchida, K. Nakamura, Y. Ando, Phys. Rev. Lett. **83**, 3717 (1999).
9. D.S. Dessau, D.S. Marshall, A.G. Loeser, C.-H. Park, A.Y. Matsuura, Z.-X. Shen, P. Fournier, A. Kapitulnik, K. Kishio, J. Eckstein, I. Bozovic, J. Electron. Spectros. Relat. Phenom. **78**, 167 (1996).
10. I. Vobornik, S. La Rosa, F. Zwick, H. Berger, M. Grioni, G. Margaritondo, R.J. Kelley, J. Ma, A. Chubukov, M. Onellion, Helv. Phys. Acta **69**, 225 (1996).
11. H. Ding, T. Yokoya, J.C. Campuzano, T. Takahashi, M. Randeria, M.R. Norman, T. Mochiku, K. Kadowaki, J. Giapintzakis, Nature **382**, 51 (1996).
12. H. Ding, M.R. Norman, T. Yokoya, T. Takeuchi, M. Randeira, J.C. Campuzano, T. Takahashi, T. Mochiku, K. Kadowaki, Phys. Rev. Lett. **78**, 2628 (1997).
13. J.M. Luttinger, Phys. Rev. **119**, 1153 (1960).
14. D.S. Marshall, D.S. Dessau, A.G. Loeser, C.-H. Park, A.Y. Matsuura, J.N. Eckstein, I. Bozovic, P. Fournier, A. Kapitulnik, W.E. Spicer, Z.-X. Shen, Phys. Rev. Lett. **76**, 4841 (1996).
15. N.L. Saini, J. Avila, A. Bianconi, A. Lanzara, M.C. Asensio, S. Tajima, G.D. Gu, N. Koshizuka, Phys. Rev. Lett. **79**, 3467 (1997).
16. J. Osterwalder, P. Aebi, P. Schwaller, L. Schlapbach, M. Shimoda, T. Mochiku, K. Kadowaki, Appl. Phys. A **60**, 247 (1995).
17. P. Schwaller, P. Aebi, H. Berger, C. Beeli, J. Osterwalder, L. Schlapbach, J. Electron. Spectros. Relat. Phenom. **76**, 127 (1995).
18. A. Yamamoto, M. Onoda, E. Takayama-Muromachi, F. Izumi, Phys. Rev. B **42**, 165 (1989).
19. A. Kampf, J.R. Schrieffer, Phys. Rev. B **41**, 6399 (1990).
20. J.R. Schrieffer, A. Kampf, Phys. Rev. B **42**, 7967 (1990).
21. H. Ding, A.F. Bellman, J.C. Campuzano, M. Randeira, M.R. Norman, T. Yokoya, H. Katayama-Yoshida, T. Mochiku, K. Kadowaki, G. Jennings, G.P Brivio, Phys. Rev. Lett. **76**, 1533 (1996).
22. S. Chakravarty, Phys. Rev. Lett. **74**, 1885 (1995).
23. D.J. Singh, W.E. Pickett, Phys. Rev. B **51**, 3128 (1995).
24. A.B. Bykov, L.N. Demmianets, J. Cryst. Growth **139**, 81 (1994).
25. W.A. Groen, D.M. de Leeuw, L.F. Feiner, Physica C **165**, 55 (1990).
26. L. Mihaly, C. Kendziora, J. Hartge, D. Mandrus, L. Forró, Rev. Sci. Instrum. **64**, 2397 (1993).
27. P. Schwaller, Ph.D. thesis, University of Zürich, 1997.
28. epo-tek 417, distributed in Switzerland by Polyscience AG, CH-6330 Cham.
29. L.L. Miller, X.L. Wang, S.X. Wang, C. Stassis, D.C. Johnston, J. Faber Jr., C.-K. Loong, Phys. Rev. B **41**, 1921 (1990).
30. S. Hüfner, *Photoelectron Spectroscopy*, 2nd edn. (Springer, Berlin, 1996).
31. T. Greber, O. Raetzo, T.J. Kreutz, P. Schwaller, W. Deichmann, E. Wetli, J. Osterwalder, Rev. Sci. Instrum. **68**, 4549 (1997).
32. M. Shimoda, T. Greber, J. Osterwalder, L. Schlapbach, Physica C **196**, 236 (1992).
33. P.A.P. Lindberg, I. Lindau, W.E. Spicer, Phys. Rev. B **40**, 6822 (1989).
34. P. Schwaller, S. Berner, T. Greber, J. Osterwalder, H. Berger, Appl. Phys. Lett. **74**, 1877 (1999).
35. F. Ronning, C. Kim, D.L. Feng, D.S. Marshall, A.G. Loeser, L.L. Miller, J.N. Eckstein, I. Bozovic, Z.-X. Shen, Science **282**, 2067 (1998).
36. A. Bansil, M. Lindroos, Phys. Rev. Lett. **83**, 5154 (1999).
37. N. Trivedi, M. Randeria, Phys. Rev. Lett. **75**, 312 (1995).
38. B.O. Wells, Z.-X. Shen, A. Matsuura, D.M. King, M.A. Kastner, M. Greven, R.J. Birgenau, Phys. Rev. Lett. **74**, 964 (1995).
39. E. Dagotto, Rev. Mod. Phys. **66**, 763 (1994).
40. D.J. Scalapino, J. Phys. Chem. Solids **56**, 1669 (1995).
41. A.V. Chubukov, D.K. Morr, K.A. Shakhnovich, Philosophical Magazine B **74**, 563 (1996).
42. D. Pines, Z. für Physik B **103**, 129 (1997).
43. R.J. Birgenau, D.R. Gabbe, H.P. Jenssen, M.A. Kastner, P.J. Picone, T.R. Thurston, G. Shirane, Y. Endoh, M. Sato, K. Yamada, Y. Hidaka, M. Oda, Y. Enomoto, M. Suzuki, T. Murakami, Phys. Rev. B **38**, 6614 (1988).
44. J.M. Tranquada, P.M. Gehring, G. Shirane, S. Shamoto, M. Sato, Phys. Rev. B **46**, 5561 (1992).
45. P. Aebi, L. Schlapbach, P. Schwaller, J. Osterwalder, H. Berger, C. Beeli, in *Proceedings of the Conference on Physical Phenomena at High Magnetic Fields II, Tallahassee, Florida, May 6-9, 1995*, edited by Z. Fisk (World Scientific, Singapore, 1996), p. 440.
46. B.O. Wells (private communication).
47. J.J.M. Pothuizen, R. Eder, N.T. Hien, M. Matoba, A.A. Menovsky, G.A. Sawatzky, Phys. Rev. Lett. **78**, 717 (1997).
48. S. LaRosa, I. Vobornik, F. Zwick, H. Berger, M. Grioni, G. Margaritondo, R.J. Kelley, M. Onellion, A. Chubukov, Phys. Rev. B **56**, 525R (1997).